JACS
JOURNAL OF THE AMERICAN CHEMICAL SOCIETY
Communication
pubs.acs.org/JACS

Growth of Alloy $MoS_{2x}Se_{2(1-x)}$ Nanosheets with Fully Tunable Chemical Compositions and Optical Properties

Honglai Li,[†] Xidong Duan,[†] Xueping Wu,[†] Xiujuan Zhuang,[†] Hong Zhou,[†] Qinglin Zhang,[†] Xiaoli Zhu,[†] Wei Hu,[†] Pinyun Ren,[†] Pengfei Guo,[†] Liang Ma,[†] Xiaopeng Fan,[†] Xiaoxia Wang,[†] Jinyou Xu,[†] Anlian Pan,*[,†] and Xiangfeng Duan*[,‡]

[†]Key Laboratory for Micro-Nano Physics and Technology of Hunan Province, State Key Laboratory of Chemo/Biosensing and Chemometrics, Hunan University, Changsha, Hunan 410082, P. R. China

[‡]Department of Chemistry and Biochemistry and California NanoSystems Institute, University of California at Los Angeles, Los Angeles, California 90095, United States

Supporting Information

ABSTRACT: Band gap engineering of atomically thin two-dimensional layered materials is critical for their applications in nanoelectronics, optoelectronics, and photonics. Here we report, for the first time, a simple one-step chemical vapor deposition approach for the simultaneous growth of alloy $MoS_{2x}Se_{2(1-x)}$ triangular nanosheets with complete composition tunability. Both the Raman and the photoluminescence studies show tunable optical properties consistent with composition of the alloy nanosheets. Importantly, all samples show a single bandedge emission peak, with the spectral peak position shifting from 668 nm (for pure MoS_2) to 795 nm (for pure $MoSe_2$), indicating the high quality for these complete composition alloy nanosheets. These band gap engineered 2D structures could open up an exciting opportunity for probing their fundamental physical properties in 2D and may find diverse applications in functional electronic/optoelectronic devices.

Transition-metal dichalcogenides (TMDs), such as MoS_2, $MoSe_2$, WS_2, and WSe_2, have recently attracted considerable interest as a new class of atomically thin two-dimensional layered materials (2DLMs), due to their atomically thin geometry, unique electronic and optical properties, and potential application integrated nanosystems.[1−20] Unlike graphene with a zero bandgap, these atomically thin 2D materials possess direct bandgaps[21] and could give light emission at room temperature, which is important for both electronic and optoelectronic applications. For MoS_2 and $MoSe_2$, the direct bandgaps are 1.856 and 1.557 eV, respectively. To precisely control the band gap of these 2DLMs is of central importance for creating optoelectronic devices with tunable spectral responses. Considering similarities in the atomic structure of these two materials, it is possible to create a mixed alloy system with a tunable band gap by alloy composition.

Alloying semiconductors with different bandgaps have been widely used in the bandgap engineering of bulk semiconductors. For applications in nanoelectronics and nanophotonics, it is very important to achieve semiconductor nanostructures with continuously tuned bandgaps. Recent advances in 0D and 1D ternary semiconductor structures have shown that their bandgaps and light emissions can be tuned gradually by changing their constituent stoichiometries,[22,23] while such studies are few for atomically thin 2D systems. Theoretical calculations have shown that 2D alloys, such as mixed ternary $MoS_2/MoSe_2/MoTe_2$ compounds, are thermodynamically stable at room temperature, and their composition may be continuously tuned between the constituent limits.[24] Very recently, composition-dependent $Mo_{1-x}W_xS_2$ monolayers have been achieved by exfoliating strategy.[25] For the broad applications in integrated devices and systems, direct growth of these bandgap engineered 2D structures should be very important. However, the growth of these composition controlled atomically thin 2D semiconductors has not been realized to date, to the best of our knowledge. Here, using a simple one-step physical evaporation process, we realized for the first time the simultaneous synthesis of complete composition ternary $MoS_{2x}Se_{2(1-x)}$ alloy nanosheets. Structural and optical investigations demonstrated that these achieved 2D semiconductors are of all high crystalline quality and exhibit composition-dependent bandedge emission, with the peak wavelength continuously tunable from around 668 nm (for pure MoS_2) to 795 nm (for pure $MoSe_2$).

The complete composition $MoS_{2x}Se_{2(1-x)}$ nanosheets were synthesized through an improved CVD route,[26] where a temperature gradient is applied for the composition selection and spatial separation which was well used for the growth of composition tunable chalcogenide alloy nanowires in the previous reports.[27,28] To prepare the ternary $MoS_{2x}Se_{2(1-x)}$ nanosheets, an alumina boat loaded with MoO_3 powder was placed into the heating zone of a quartz tube (Figure S1), and another two boats loaded with sulfur and selenium powder were placed at the upstream. Several pieces of Si substrates (with 300 nm SiO_2) were placed on the alumina boat with MoO_3 powder. Before heating, an Ar flow was introduced into the system, to ensure a favorable circumstance for the synthesis of the sample. The furnace was then rapidly heated to 830 °C and maintained at this temperature for 8 min, keeping the

Received: January 4, 2014
Published: February 24, 2014

 © 2014 American Chemical Society dx.doi.org/10.1021/ja500069b | J. Am. Chem. Soc. 2014, 136, 3756−3759

pressure inside the tube at 8 Torr. $MoS_{2x}Se_{2(1-x)}$ nanosheets with gradually changed composition were deposited on different positions of SiO_2 surfaces along the length of the tube.

A typical scanning electron microscopy (SEM) image of a representative sample shows that the achieved structures are triangular nanosheets with the edge lengths of 30−80 μm (Figure 1a). Atomic Force Microscopy (AFM) studies reveal

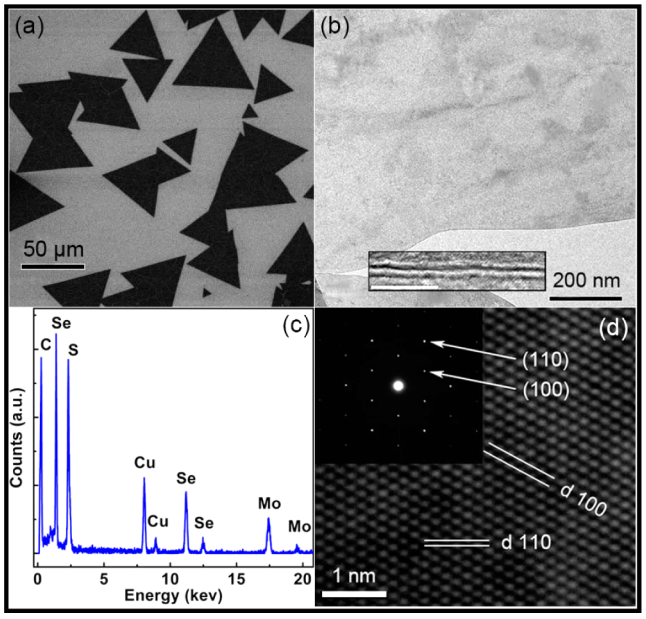

Figure 1. (a) Typical SEM morphology of the obtained ternary $MoS_{2x}Se_{2(1-x)}$ nanosheets. (b) TEM image of a part of a single ternary nanosheet and a cross-section image edge (inset, scale bar 5 nm). (c) Corresponding TEM-EDX profile of the sample. (d) HRTEM image taken from (b) and its SAED pattern (inset).

that most of these triangular nanosheets have a thickness in range of 1.65−2.29 nm (see Figure S2), corresponding to bilayer to trilayer materials. Transmission electron microscopy (TEM) combined with energy-dispersive X-ray spectroscopy (EDS) were used to investigate the microstructure and elemental composition of these nanosheets. Figure 1b shows the TEM image of a typical nanosheet, which is broken partly. The inset of Figure 1b is the cross-section image of the sample, where the distance of the two parallel dark lines was measured with a spacing of ~6.75 Å, consistent with the layer separation of $MoS_{2x}Se_{2(1-x)}$ material. The EDX spectrum shown in Figure 1c demonstrates that the nanosheet consists of Mo, S, and Se elements (the exhibited C and Cu elements are from the grid of copper), with the S mole fraction [x, S/(S + Se)] of ~0.48, indicating the composition of the nanosheet as $MoS_{2(0.48)}Se_{2(0.52)}$. The EDX results of other representative samples with different compositions are shown in Figure S3. Figure 1d gives the corresponding high-resolution TEM (HRTEM) image of the nanosheet, which demonstrates the single-crystalline nature of the 2D structures, with a lattice spacing of 0.278 and 0.161 nm, in agreement with the (100) and (110) planes of the previously obtained $MoS_{2(0.48)}Se_{2(0.52)}$ composition from the EDX analysis. The selected area electron diffraction (SAED) pattern of the nanosheet (inset of Figure 1d) displays the lattice arrangement, further demonstrating the high-quality hexagonal symmetry structures of these achieved $MoS_{2x}Se_{2(1-x)}$ nanosheets.

Raman spectra can be used to characterize the composition dependent vibration modes of these alloy nanosheets.[29] Figure 2a shows the normalized Raman spectra of the as-grown

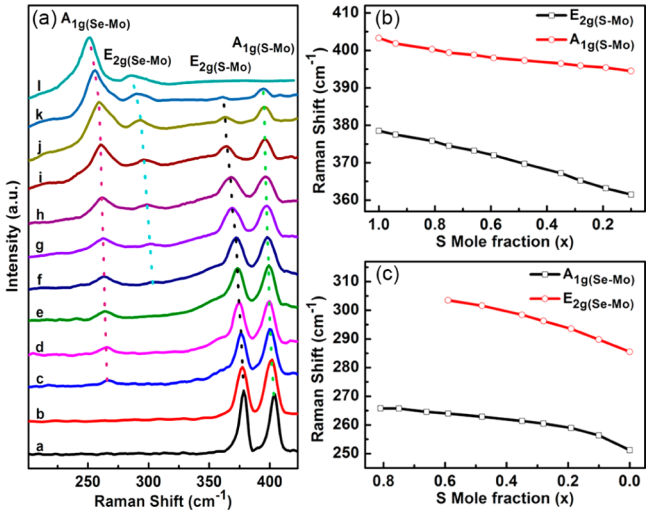

Figure 2. (a) Raman spectrum of the $MoS_{2x}Se_{2(1-x)}$ nanosheets excited with a 488 nm argon ion laser. (b,c) S−Mo related modes [$E_{2g(S-Mo)}$, $A_{1g(S-Mo)}$] and Se−Mo related modes [$A_{1g(Se-Mo)}$, $E_{2g(Se-Mo)}$] shift with S mole fraction decreases.

$MoS_{2x}Se_{2(1-x)}$ nanosheets with composition x decreased gradually from 1 (down-most, pure MoS_2) to 0 (upmost, pure $MoSe_2$) excited with a 488 nm argon ion laser, respectively. Most of the curves exhibit four modes, assigned to the molecular vibration modes $A_{1g(Se-Mo)}$, $E_{2g(Se-Mo)}$, $E_{2g(S-Mo)}$ and $A_{1g(S-Mo)}$, respectively. From the curves a to l, the intensity of the S−Mo related modes [$E_{2g(S-Mo)}$, $A_{1g(S-Mo)}$] gradually decrease until they completely disappear, while the Se−Mo related modes [$A_{1g(Se-Mo)}$, $E_{2g(Se-Mo)}$] are absent or very weak at the initial stage and gradually come into appearance with the corresponding intensity increased.

These molecular vibration mode transitions show good agreements with the gradual decreased(increased) S(Se) contents in these composition modulated $MoS_{2x}Se_{2(1-x)}$ alloys. At the same time, as shown in Figure 2b,c, with decreasing the S molar fraction (from curves a to l), all the vibration modes (both the S−Mo related and the Se−Mo related) shift to low frequency. As shown in Figure 2a, the Se−Mo related and the S−Mo related modes are located at low and high frequencies, respectively. With the increase of the Se content (from curves a to l), the interactions between S and Se atoms would soften the S−Mo related modes and decrease their vibration frequency, and at the same time the Se−Mo related vibrations would also shift to the lower frequency as the effect of S atoms becoming less and less until they arrive at the original mode positions of the binary $MoSe_2$ compound.

Figure 3a shows the normalized photoluminescence (PL) spectra of the obtained composition modulated $MoS_{2x}Se_{2(1-x)}$ nanosheets excited with a 488 nm argon ion laser. Curves (a−l) are for the $MoS_{2x}Se_{2(1-x)}$ nanosheets collected at temperature of 830 to 796 °C, respectively, as shown in Figure 3b, where the substrate position-dependent growth temperature and S molar fraction (x) of the achieved nanosheets were given. All the samples show single emission bands, with the spectral peaks continuously shifted from 668 nm (for pure MoS_2) to 795 nm (for pure $MoSe_2$), which is consistent to the band edge

dx.doi.org/10.1021/ja500069b | J. Am. Chem. Soc. 2014, 136, 3756−3759

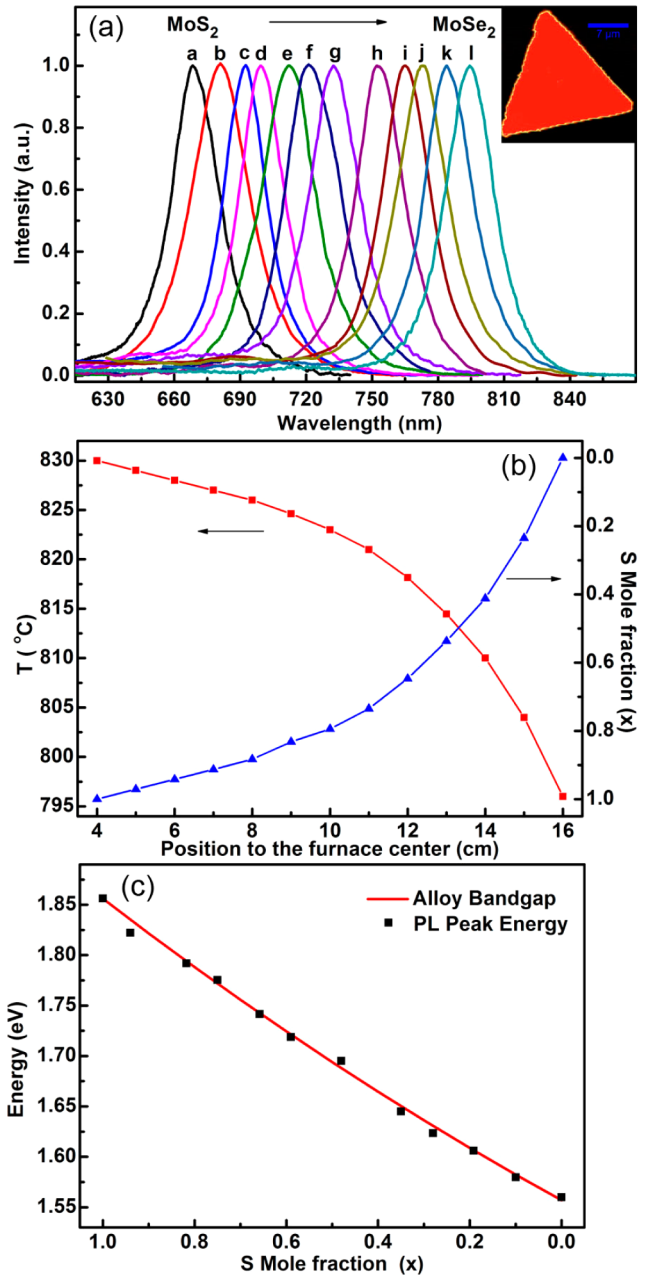

Figure 3. (a) PL spectrum of the complete composition $MoS_{2x}Se_{2(1-x)}$ nanosheets and a typical PL mapping of a single ternary nanosheet (the inset, scale bar, 7 um) excited with a 488 argon ion laser. (b) Substrate position-dependent growth temperature and S molar fraction (x) of the achieved nanosheets and (c) composition-dependent (x) bandgaps of the achieved nanosheets.

transitions of ternary $MoS_{2x}Se_{2(1-x)}$ thin films.[11,12] Figure 3c gives the composition-dependent (x) bandgaps of the achieved nanosheets. The solid line is the fitted values from the bandgap relation for ternary semiconductor alloys:

$$E_g(x) = xE_g(MoS_2) + (1 - x)E_g(MoSe_2) - bx(1 - x) \quad (1)$$

Here $E_g(MoS_2)$ is 1.856 eV and $E_g(MoSe_2)$ is 1.557 eV. And the band gap bowing parameter b = 0.05.[30] The dots are the experiment results obtained from PL peak position and EDX composition analysis. Significantly, the experimental data are well consistent with the prediction based on eq 1, demonstrating that the observed single PL emissions are all originated from the bandedge emission, without any observed defect-related emission bands. The inset of Figure 3a is a PL mapping of a representative single ternary nanosheet, which shows that the light emission is very uniform across the whole microstructure. Together, these optical studies further demonstrate the complete composition $MoS_{2x}Se_{2(1-x)}$ nanosheets exhibit high-quality optical properties, which are in good agreements with the structural and composition investigations described above.

In summary, atomically thin uniform 2D $MoS_{2x}Se_{2(1-x)}$ nanosheets have been simultaneously synthesized with complete composition ($0 \leq x \leq 1$) tunability using a very simple one-step temperature gradient assisted CVD route. The achieved samples exhibit triangular shape with edge length up to 80 μm. Under laser excitation, the nanosheets collected from difference growth temperature (different positions along the length of the tube) show a consistent composition-related Raman shift and PL emission. The nanosheets with variable compositions all show single bandedge emission band, with the spectral peak continuously tunable from ~668 nm (for pure MoS_2) to ~795 nm (for pure $MoSe_2$). These achieved 2D alloy nanostructures with high-quality crystallization could find significant applications in tunable nanoscale photoelectric devices at the near-infrared range.

■ ASSOCIATED CONTENT

Supporting Information

The experiment details and and characterization data. This material is available free of charge via the Internet at http://pubs.acs.org.

■ AUTHOR INFORMATION

Corresponding Authors

anlian.pan@hnu.edu.cn
xduan@chem.ucla.edu

Notes

The authors declare no competing financial interest.

■ ACKNOWLEDGMENTS

We are grateful to the National Basic Research Program of China (no. 2012CB932703), the NSF of China (nos.11374092 and 11204073), and the Research Fund for the Doctoral Program of Higher Education (nos. 20110161110034 and 20110161120027) for financial support.

■ REFERENCES

(1) Halim, U.; Zheng, C. R.; Chen, Y.; Lin, Z.; Jiang, S.; Cheng, R.; Huang, Y.; Duan, X. *Nat. Comm.* **2013**, *4*, 2213.
(2) Yu, W. J.; Liu, Y.; Zhou, H.; Yin, A.; Li, Z.; Huang, Y.; Duan, X. *Nat. Nanotechnol.* **2013**, *8*, 952.
(3) Yu, W. J.; Li, Z.; Zhou, H.; Chen, Y.; Wang, Y.; Huang, Y.; Duan, X. *Nat. Mater.* **2013**, *12*, 246.
(4) Qiu, H.; Xu, T.; Wang, Z.; Ren, W.; Nan, H.; Ni, Z.; Chen, Q.; Yuan, S.; Miao, F.; Song, F.; Long, G.; Shi, Y.; Sun, L.; Wang, J.; Wang, X. *Nat. Comm.* **2013**, *4*, 2642.
(5) Luo, X.; Zhao, Y. Y.; Zhang, J.; Toh, M. L.; Kloc, C.; Xiong, Q. H.; Quek, S. Y. *Phys. Rev. B* **2013**, *88*, 195313.
(6) Jones, A.; Yu, H.; Ghimire, N.; Wu, S.; Aivazian, G.; Ross, J.; Zhao, B.; Yan, J.; Mandrus, D.; Xiao, D.; Yao, W.; Xu, X. *Nat. Nanotechnol.* **2013**, *8*, 634.
(7) Wu, S.; Ross, J.; Liu, G.; Aivazian, G.; Jones, A.; Fei, Z.; Zhu, W.; Xiao, D.; Yao, W.; Cobden, D.; Xu, X. *Nat. Phys.* **2013**, *9*, 149.

(8) Liu, Y.; Nan, H.; Wu, X.; Pan, W.; Wang, W.; Bai, J.; Zhao, W.; Sun, L.; Wang, X.; Ni, Z. *ACS Nano* **2013**, *7*, 4202.
(9) Huang, X.; Zeng, Z. Y.; Zhang, H. *Chem. Soc. Rev.* **2013**, *42*, 1934.
(10) Li, H.; Qi, X. Y.; Wu, J.; Zeng, Z. Y.; Wei, J.; Zhang, H. *ACS Nano* **2013**, *7*, 2842.
(11) Elías, A. L.; Perea-López, N.; Castro-Beltrán, A.; Berkdemir, A.; Lv, R.; Feng, S.; Long, A. D.; Hayashi, T.; Kim, Y. A.; Endo, M.; Gutiérrez, H. R.; Pradhan, N. R.; Balicas, L.; Mallouk, T. E.; López-Urías, F.; Terrones, H.; Terrones, M. *ACS Nano* **2013**, *7*, 5235.
(12) Wang, X.; Feng, H.; Wu, Y.; Jiao, L. *J. Am. Chem. Soc.* **2013**, *135*, 5304.
(13) Berkdemir, A.; Gutierrez, H. R.; Botello-Mendez, A. R.; Perea-Lopez, N.; Elias, A. L.; Chia, C. I.; Wang, B.; Crespi, V. H.; Lopez-Urias, F.; Charlier, J. C.; Terrones, H.; Terrones, M. *Sci. Rep.* **2013**, *3*, 1755.
(14) Wang, C.; Cheng, R.; Liao, L.; Duan, X. *Nano Today* **2013**, *8*, 514.
(15) Liu, J.; Zeng, Z.; Cao, X.; Lu, G.; Wang, L.; Fan, Q.; Huang, W.; Zhang, H. *Small* **2012**, *8*, 3517.
(16) Yin, Z.; Li, H.; Li, H.; Jiang, L.; Shi, Y.; Sun, Y.; Lu, G.; Zhang, Q.; Chen, X.; Zhang, H. *ACS Nano* **2012**, *6*, 74.
(17) Zhou, W.; Yin, Z.; Du, Y.; Huang, X.; Zeng, Z.; Fan, Z.; Liu, H.; Wang, J.; Zhang, H. *Small* **2013**, *9*, 140.
(18) Zhu, C.; Zeng, Z.; Li, H.; Li, F.; Fan, C.; Zhang, H. *J. Am. Chem. Soc.* **2013**, *135*, 5998.
(19) He, Q.; Zeng, Z.; Yin, Z.; Li, H.; Wu, S.; Huang, X.; Zhang, H. *Small* **2012**, *8*, 2994.
(20) Li, H.; Yin, Z.; He, Q.; Li, H.; Huang, X.; Lu, G.; Fam, D. W. H.; Tok, A. l. Y.; Zhang, Q.; Zhang, H. *Small* **2012**, *8*, 63.
(21) Tongay, S.; Zhou, J.; Ataca, C.; Lo, K.; Matthews, T. S.; Li, J.; Grossman, J. C.; Wu, J. *Nano Lett.* **2012**, *12*, 5576.
(22) Bailey, R. E.; Nie, S. *J. Am. Chem. Soc.* **2003**, *125*, 7100.
(23) Liu, Y.; Zapien, J. A.; Shan, Y. Y.; Geng, C. Y.; Lee, C. S.; Lee, S. T. *Adv. Mater.* **2005**, *17*, 1372.
(24) Komsa, H.-P.; Krasheninnikov, A. V. *J. Phys. Chem. Lett.* **2012**, *3*, 3652.
(25) Chen, Y.; Xi, J.; Dumcenco, D. O.; Liu, Z.; Suenaga, K.; Wang, D.; Shuai, Z.; Huang, Y. S.; Xie, L. *ACS Nano* **2013**, *7*, 4610.
(26) Shaw, J. C.; Zhou, H.; Chen, Y.; Weiss, N. O.; Liu, Y.; Huang, Y.; Duan, X. *Nano Res.* **2014**, DOI: 10.1007/s12274-014-0417-z.
(27) Pan, A.; Liu, R.; Sun, M.; Ning, C. Z. *J. Am. Chem. Soc.* **2009**, *131*, 9502.
(28) Pan, A.; Yang, H.; Liu, R.; Yu, R.; Zou, B.; Wang, Z. *J. Am. Chem. Soc.* **2005**, *127*, 15692.
(29) Buscema, M.; Steele1, G. A.; van der Zant, H. S. J.; Castellanos-Gomez, A. *Nano Res.* **2014**, DOI: 10.1007/s12274-014-0424-0.
(30) Kang, J.; Tongay, S.; Li, J.; Wu, J. *J. Appl. Phys.* **2013**, *113*, 143703.